Scilight

*Complex Systems Stability & Control*
https://www.sciltp.com/journals/cssc



*Article*

# Global Fixed-Time Synchronization of Fractional-Order Dual-Split-Quaternion Valued Memristive Neural Networks: Full Proofs and 6D Relativistic Image Encryption

Grienggrai Rajchakit

Program in Industrial Optimisation and Applications, Faculty of Science, Maejo University, Chiang Mai 50290, Thailand; kreangkri@mju.ac.th

**How To Cite**: Rajchakit, G. Global Fixed-Time Synchronization of Fractional-Order Dual-Split-Quaternion Valued Memristive Neural Networks: Full Proofs and 6D Relativistic Image Encryption. *Complex Systems Stability & Control* **2026**, *2*(3), 2. https://doi.org/10.53941/cssc.2026.100013

Received: 1 April 2026
Revised: 28 May 2026
Accepted: 29 May 2026
Published: 7 July 2026

**Abstract:** This paper advances hypercomplex neural-network theory by introducing Dual-Split-Quaternion (DSQ) algebra for control and synchronization. Whereas standard quaternions model only three-dimensional Euclidean rotations, DSQ algebra combines a nilpotent dual unit ($\epsilon^2 = 0$) with split-quaternion bases ($i^2 = -1$, $j^2 = 1$, $k^2 = 1$), making it suitable for coupled non-Euclidean rotational and translational representations. These algebraic properties also introduce zero-divisors, non-compactness, and nilpotent degeneracy, which invalidate conventional Lyapunov metric constructions. To address this issue, we establish a rigorous framework for Fractional-Order Dual-Split-Quaternion Valued Memristive Neural Networks (FODSQVMNNs) with constant transmission delays, and we prove an absolute composite norm inequality in DSQ space. Using Filippov differential inclusions for memristive switching, we synthesize an event-triggered fixed-time sliding-mode controller. The resulting analysis guarantees synchronization within a computable fixed time $T_{\max}$ that is independent of initial conditions. Comparative tables and embedded mathematical simulations validate the theoretical and computational advantages of the proposed framework. Finally, synchronized non-compact 16-dimensional hyperchaotic attractors generated from coupled DSQ states are leveraged to construct a 6D relativistic color-image encryption scheme with strong resistance to statistical and differential attacks.

**Keywords:** dual-split-quaternion; memristive neural networks; fractional calculus; fixed-time synchronization; filippov inclusion; relativistic encryption

## 1. Introduction

The evolution of artificial neural networks has transcended the real domain, moving rapidly into multidimensional hypercomplex algebras to process highly correlated spatiotemporal data [1,2]. Standard Quaternion-Valued Neural Networks (QVNNs) effectively model three-dimensional Euclidean rotations and have been applied to robotic attitude representation, color image processing, and multidimensional signal analysis [3,4]. However, standard quaternions alone do not directly encode translational degrees of freedom or pseudo-Euclidean geometric signatures. Translation is naturally represented by dual-number constructions, while split-quaternion algebra is associated with indefinite metric structures and Lorentz-type geometry [5–7]

Memristive neural networks provide an additional modeling advantage because a memristor has a state-dependent resistance and can describe switching, hysteresis, and synaptic plasticity effects. The memristor concept was originally introduced as the missing circuit element, and it has since become a useful mathematical tool for neural-network models with discontinuous state-dependent couplings [8]. In such systems, abrupt switching of memristive weights is commonly treated through Filippov differential inclusions, which replace discontinuous right-hand sides with set-valued convexified maps [9]. When these networks are further combined with fractional-order calculus, the state evolution captures hereditary memory and nonlocal dynamics, which are important in many complex biological and physical systems [10,11].

Dual-Split-Quaternion (DSQ) algebra merges the nilpotent dual unit ($\epsilon^2 = 0$) with split-quaternion bases

($i^2 = -1$, $j^2 = 1$, $k^2 = 1$). A single DSQ element contains two split-quaternion components and therefore has an eight-real-coefficient representation. In the encryption application of this paper, two coupled synchronized DSQ states are used to generate a 16-dimensional hyperchaotic coefficient sequence. This construction is useful for six-channel encryption because it supplies both color-channel streams and spatial-permutation streams.

Despite these advantages, mathematically controlling FODSQVMNNs presents several theoretical barriers. The DSQ algebra is not a division algebra; it contains zero-divisors and nilpotent components. Consequently, a conventional quadratic norm or pseudo-norm may become zero or fail to capture growth in the dual component. These features can invalidate standard Lyapunov metric arguments. Furthermore, continuous communication-based synchronization is impractical in high-dimensional non-compact models. Event-triggered fixed-time control is therefore desirable because it reduces actuation while preserving convergence within a uniform time bound independent of initial conditions [12].

Recent studies published in 2025 and 2026 show that synchronization of hypercomplex and fractional-order neural networks remains an active research direction. Quaternion-valued memristive neural networks with time-varying delays and impulsive effects were studied in [13], while delayed Clifford-valued neural networks with a D-operator and aperiodic semi-intermittent control were investigated in [14]. A fast fixed-/preassigned-time synchronization method for Clifford-valued neural networks with medical image encryption was proposed in [15]. For fractional quaternion-valued systems, finite-time synchronization with discontinuous activations and uncertainties was examined in [16], and delayed fractional-order quaternion-valued neural networks were further studied through a matrix-negative-definition approach in [17]. Recent works on coupled memristive networks and fractional fuzzy cellular neural networks further confirm the importance of fixed-time design, actuator limitations, and robust delay compensation [18, 19]. These contributions motivate the present study but do not address the simultaneous presence of nilpotent dual components, split-quaternion zero-divisors, memristive Filippov switching, event-triggered fixed-time control, and 6D encryption within one DSQ framework.

Novel Contributions of this Manuscript:

1. FODSQVMNN formulation: We define a fractional-order memristive neural network operating in the non-commutative, nilpotent, non-compact DSQ space with constant transmission delays.
2. DSQ absolute composite metric: We introduce and prove a composite norm inequality that avoids the zero-divisor and nilpotent collapse of the standard pseudo-norm.
3. Rigorous event-triggered fixed-time control: We derive the synchronization error system explicitly, formulate an event-triggered sliding-mode controller, and present theorem conditions for global fixed-time synchronization and Zeno exclusion.
4. 6D image encryption: We map synchronized 16-dimensional DSQ hyperchaotic sequences to six encryption streams associated with $(R, G, B, \alpha, X, Y)$, and provide explicit encryption and decryption procedures.

## 2. Notation and Algebraic Foundations

### *2.1. Notation*

The following notation is used throughout the paper. $\mathbb{R}$ denotes the set of real numbers. $\mathbb{SQ}$ denotes the split-quaternion algebra

$$\mathbb{SQ} = \{x_0 + x_1 i + x_2 j + x_3 k : x_n \in \mathbb{R},\ i^2 = -1,\ j^2 = k^2 = 1\}, \tag{1}$$

with multiplication rules $ij = k = -ji$, $jk = -i = -kj$, and $ki = j = -ik$. $\mathbb{DSQ}$ denotes the dual-split-quaternion algebra

$$\mathbb{DSQ} = \{q = q_p + \epsilon q_d : q_p, q_d \in \mathbb{SQ},\ \epsilon \neq 0,\ \epsilon^2 = 0\}. \tag{2}$$

For $q = q_p + \epsilon q_d \in \mathbb{DSQ}$, the primal and dual components are written as

$$q_p = \sum_{n=0}^{3} q_{p,n} e_n, \qquad q_d = \sum_{n=0}^{3} q_{d,n} e_n, \tag{3}$$

where $e_0 = 1$, $e_1 = i$, $e_2 = j$, and $e_3 = k$. Thus $q_{p,n}$ and $q_{d,n}$ are real coefficients. The coefficient-vector map is denoted by

$$\chi(q) = (q_{p,0}, q_{p,1}, q_{p,2}, q_{p,3}, q_{d,0}, q_{d,1}, q_{d,2}, q_{d,3})^T \in \mathbb{R}^8. \tag{4}$$

For a DSQ-valued vector $x = (x_1, \ldots, x_N)^T \in \mathbb{DSQ}^N$, the notation $\chi_N(x) = (\chi(x_1)^T, \ldots, \chi(x_N)^T)^T$ is used. The symbols ${}_{t_0}^{C}D_t^{\alpha}$ and ${}_{t_0}I_t^{1-\alpha}$ denote the Caputo fractional derivative and the Riemann-Liouville fractional

integral, respectively, with $0 < \alpha < 1$. The constants $L_s$ and $M_s$ are Lipschitz constants for activation functions $f_s$ and $g_s$, while $M_{fs}$ and $M_{gs}$ denote uniform bounds of these activation functions on the considered operating set.

### *2.2. Preliminaries of DSQ Algebra*

A dual-split-quaternion $q \in \mathbb{DSQ}$ is defined as

$$q = q_p + \epsilon q_d, \tag{5}$$

where $q_p, q_d \in \mathbb{SQ}$ and $\epsilon$ is the nilpotent dual unit satisfying $\epsilon \neq 0$ and $\epsilon^2 = 0$. Because $j^2 = 1$ and $k^2 = 1$, $\mathbb{SQ}$ and $\mathbb{DSQ}$ contain zero-divisors. For example, $(1 + j)(1 - j) = 1 - j^2 = 0$.

For $p, q \in \mathbb{DSQ}$, multiplication is non-commutative and is given by

$$pq = (p_p + \epsilon p_d)(q_p + \epsilon q_d) = p_p q_p + \epsilon(p_p q_d + p_d q_p), \tag{6}$$

where the $p_d q_d$ term vanishes because $\epsilon^2 = 0$.

### *2.3. Absolute Composite Norm and DSQ Sign Function*

The standard quadratic form associated with a split-quaternion can be zero or negative and does not provide a positive-definite Lyapunov metric for the dual component. We therefore use the following absolute composite norm.

**Definition 1** (Absolute composite DSQ norm)**.** *For any $q = q_p + \epsilon q_d \in \mathbb{DSQ}$, define*

$$\|q\|_{\mathbb{DSQ}} = \|q_p\|_a + \|q_d\|_a = \sqrt{\sum_{n=0}^{3} q_{p,n}^2} + \sqrt{\sum_{n=0}^{3} q_{d,n}^2}, \tag{7}$$

*where $\|\cdot\|_a$ is the Euclidean norm of the corresponding split-quaternion coefficient vector. For $x = (x_1, \ldots, x_N)^T \in \mathbb{DSQ}^N$, define $\|x\|_{1,\mathbb{DSQ}} = \sum_{r=1}^{N} \|x_r\|_{\mathbb{DSQ}}$.*

**Definition 2** (Coefficient sign map)**.** *For $q = q_p + \epsilon q_d \in \mathbb{DSQ}$, define the coefficient sign vector*

$$\sigma(q) = \left(\sigma_p(q)^T, \sigma_d(q)^T\right)^T \in \mathbb{R}^8, \tag{8}$$

*where*

$$\sigma_p(q) = \begin{cases} (q_{p,0}, q_{p,1}, q_{p,2}, q_{p,3})^T / \|q_p\|_a, & q_p \neq 0, \\ 0, & q_p = 0, \end{cases} \tag{9}$$

$$\sigma_d(q) = \begin{cases} (q_{d,0}, q_{d,1}, q_{d,2}, q_{d,3})^T / \|q_d\|_a, & q_d \neq 0, \\ 0, & q_d = 0. \end{cases} \tag{10}$$

*For $x \in \mathbb{DSQ}^N$, $\sigma_N(x) = (\sigma(x_1)^T, \ldots, \sigma(x_N)^T)^T$. Therefore, expressions such as $\mathrm{sgn}(x)^T\, {}_{t_0}^{C}D_t^{\alpha} x$ are understood as real scalar coefficient-vector inner products, namely*

$$\sigma_N(x)^T \chi_N \left({}_{t_0}^{C}D_t^{\alpha} x\right). \tag{11}$$

*This convention avoids mixing DSQ-valued products with real scalar inequalities.*

**Lemma 1** (Split-quaternion product bound)**.** *For any $x, y \in \mathbb{SQ}$,*

$$\|xy\|_a \leq 2 \|x\|_a \|y\|_a. \tag{12}$$

**Proof.** Let $x = x_0 + x_1 i + x_2 j + x_3 k$ and $y = y_0 + y_1 i + y_2 j + y_3 k$. From the split-quaternion multiplication rules,

$$
\begin{aligned}
xy &= z_0 + z_1 i + z_2 j + z_3 k, \\
z_0 &= x_0 y_0 - x_1 y_1 + x_2 y_2 + x_3 y_3, \\
z_1 &= x_0 y_1 + x_1 y_0 - x_2 y_3 + x_3 y_2, \\
z_2 &= x_0 y_2 - x_1 y_3 + x_2 y_0 + x_3 y_1, \\
z_3 &= x_0 y_3 + x_1 y_2 - x_2 y_1 + x_3 y_0.
\end{aligned} \tag{13}
$$

Each $z_n$ is the inner product of the coefficient vector $(x_0, x_1, x_2, x_3)^T$ with a signed permutation of $(y_0, y_1, y_2, y_3)^T$. Hence, by the Cauchy-Schwarz inequality, $|z_n| \leq \|x\|_a \|y\|_a$ for $n = 0, 1, 2, 3$. Therefore,

$$
\|xy\|_a^2 = \sum_{n=0}^{3} z_n^2 \leq 4 \|x\|_a^2 \|y\|_a^2 , \tag{14}
$$

which proves (12). □

**Lemma 2** (Nilpotent-split norm inequality)**.** *For any $p, q \in \mathbb{DSQ}$, the absolute composite norm satisfies*

$$
\|pq\|_{\mathbb{DSQ}} \leq 4 \|p\|_{\mathbb{DSQ}} \|q\|_{\mathbb{DSQ}} . \tag{15}
$$

**Proof.** Using (6), the triangle inequality, and Lemma 1,

$$
\begin{aligned}
\|pq\|_{\mathbb{DSQ}} &= \|p_p q_p\|_a + \|p_p q_d + p_d q_p\|_a \\
&\leq \|p_p q_p\|_a + \|p_p q_d\|_a + \|p_d q_p\|_a \\
&\leq 2 \|p_p\|_a \|q_p\|_a + 2 \|p_p\|_a \|q_d\|_a + 2 \|p_d\|_a \|q_p\|_a .
\end{aligned} \tag{16}
$$

On the other hand,

$$
\begin{aligned}
4 \|p\|_{\mathbb{DSQ}} \|q\|_{\mathbb{DSQ}} &= 4(\|p_p\|_a + \|p_d\|_a)(\|q_p\|_a + \|q_d\|_a) \\
&= 4 \|p_p\|_a \|q_p\|_a + 4 \|p_p\|_a \|q_d\|_a + 4 \|p_d\|_a \|q_p\|_a + 4 \|p_d\|_a \|q_d\|_a .
\end{aligned} \tag{17}
$$

Since all norm terms in (17) are nonnegative, comparison of (16) and (17) yields (15). □

### *2.4. Fixed-Time Stability Lemmas*

**Lemma 3** (Fractional fixed-time stability)**.** *For a continuous Lyapunov function $V(t) \geq 0$, if*

$$
{}_{t_0}^{C} D_t^{\alpha} V(t) \leq -\mu_1 V^m(t) - \mu_2 V^n(t), \tag{18}
$$

*where $\mu_1, \mu_2 > 0$, $m > 1$, and $0 < n < 1$, then the system converges to the origin in a globally fixed time satisfying*

$$
T_{\max} \leq \frac{\Gamma(1+\alpha)}{\mu_1 (m-1)} + \frac{\Gamma(1+\alpha)}{\mu_2 (1-n)}, \tag{19}
$$

*which is independent of the initial value $V(t_0)$.*

**Lemma 4** (Fractional derivative of the absolute DSQ norm)**.** *Let $x(t) = (x_1(t), \ldots, x_N(t))^T \in \mathbb{DSQ}^N$ be componentwise absolutely continuous. Then*

$$
{}_{t_0}^{C} D_t^{\alpha} \|x(t)\|_{1,\mathbb{DSQ}} \leq \sigma_N(x(t))^T \chi_N \left( {}_{t_0}^{C} D_t^{\alpha} x(t) \right) . \tag{20}
$$

*In particular, for a single DSQ component $q(t)$,*

$$
{}_{t_0}^{C} D_t^{\alpha} \|q(t)\|_{\mathbb{DSQ}} \leq \sigma(q(t))^T \chi \left( {}_{t_0}^{C} D_t^{\alpha} q(t) \right) . \tag{21}
$$

**Proof.** The mapping $q \mapsto \|q\|_{\mathbb{DSQ}} = \|q_p\|_a + \|q_d\|_a$ is convex as a sum of Euclidean norms of real coefficient

vectors. Its subgradient at $q$ is represented by the coefficient sign vector $\sigma(q)$ in Definition 2. Applying the standard subgradient inequality to the componentwise Caputo derivative gives the desired scalar inequality. Summing over $r = 1, \ldots, N$ proves (20). □

## 3. System Formulation and Filippov Inclusion

The $N$-dimensional FODSQVMNN drive system with constant transmission delay $\tau > 0$ is defined over $\mathbb{DSQ}$ as

$$ {}^{C}_{t_0}D^{\alpha}_{t} x_r(t) = -c_r x_r(t) + \sum_{s=1}^{N} a_{rs}(x_r(t)) f_s(x_s(t)) + \sum_{s=1}^{N} b_{rs}(x_r(t)) g_s(x_s(t-\tau)) + I_r, \tag{22} $$

where $x_r(t) \in \mathbb{DSQ}$, $c_r > 0$, $I_r \in \mathbb{DSQ}$, and $r = 1, \ldots, N$. The memristive connection weights are

$$ a_{rs}(x_r) = \begin{cases} \hat{a}_{rs}, & \|x_r\|_{\mathbb{DSQ}} \le \Upsilon_r, \\ \check{a}_{rs}, & \|x_r\|_{\mathbb{DSQ}} > \Upsilon_r, \end{cases} \tag{23} $$

$$ b_{rs}(x_r) = \begin{cases} \hat{b}_{rs}, & \|x_r\|_{\mathbb{DSQ}} \le \Upsilon_r, \\ \check{b}_{rs}, & \|x_r\|_{\mathbb{DSQ}} > \Upsilon_r, \end{cases} \tag{24} $$

where $\hat{a}_{rs}$, $\check{a}_{rs}$, $\hat{b}_{rs}$, and $\check{b}_{rs}$ are DSQ-valued constants. The switching jumps are explicitly defined as

$$ \Delta a_{rs} = \check{a}_{rs} - \hat{a}_{rs}, \qquad \Delta b_{rs} = \check{b}_{rs} - \hat{b}_{rs}. \tag{25} $$

Thus a switching jump occurs when $\|x_r\|_{\mathbb{DSQ}}$ crosses the threshold $\Upsilon_r$, causing the corresponding connection coefficient to move between the hatted and checked values.

Because the right-hand side is discontinuous at $\|x_r\|_{\mathbb{DSQ}} = \Upsilon_r$, Filippov's differential inclusion is employed. There exist measurable functions

$$ \tilde{a}^{x}_{rs}(t) \in \mathrm{co}\{\hat{a}_{rs}, \check{a}_{rs}\}, \qquad \tilde{b}^{x}_{rs}(t) \in \mathrm{co}\{\hat{b}_{rs}, \check{b}_{rs}\} \tag{26} $$

such that the drive system is represented as

$$ {}^{C}_{t_0}D^{\alpha}_{t} x_r(t) = -c_r x_r(t) + \sum_{s=1}^{N} \tilde{a}^{x}_{rs}(t) f_s(x_s(t)) + \sum_{s=1}^{N} \tilde{b}^{x}_{rs}(t) g_s(x_s(t-\tau)) + I_r. \tag{27} $$

The response system is

$$ {}^{C}_{t_0}D^{\alpha}_{t} y_r(t) = -c_r y_r(t) + \sum_{s=1}^{N} \tilde{a}^{y}_{rs}(t) f_s(y_s(t)) + \sum_{s=1}^{N} \tilde{b}^{y}_{rs}(t) g_s(y_s(t-\tau)) + I_r + U_r(t), \tag{28} $$

where $U_r(t)$ is the control input and $\tilde{a}^{y}_{rs}(t)$, $\tilde{b}^{y}_{rs}(t)$ are the Filippov selections associated with the response system.

### *3.1. Complete Derivation of the Synchronization Error System*

Define the synchronization error

$$ e_r(t) = y_r(t) - x_r(t), \qquad r = 1, \ldots, N. \tag{29} $$

Subtracting (27) from (28) gives

$$ \begin{aligned} {}^{C}_{t_0}D^{\alpha}_{t} e_r(t) &= {}^{C}_{t_0}D^{\alpha}_{t} y_r(t) - {}^{C}_{t_0}D^{\alpha}_{t} x_r(t) \\ &= -c_r\big(y_r(t) - x_r(t)\big) + \sum_{s=1}^{N} \left[\tilde{a}^{y}_{rs}(t) f_s(y_s(t)) - \tilde{a}^{x}_{rs}(t) f_s(x_s(t))\right] \\ &\quad + \sum_{s=1}^{N} \Big[\tilde{b}^{y}_{rs}(t) g_s(y_s(t-\tau)) - \tilde{b}^{x}_{rs}(t) g_s(x_s(t-\tau))\Big] + U_r(t). \end{aligned} \tag{30} $$

Therefore,

$$
\begin{aligned}
{}_{t_0}^{C}D_t^{\alpha} e_r(t) = -c_r e_r(t) + \sum_{s=1}^{N} [\tilde{a}_{rs}^{y}(t) f_s(y_s(t)) - \tilde{a}_{rs}^{x}(t) f_s(x_s(t))] \\
+ \sum_{s=1}^{N} \left[\tilde{b}_{rs}^{y}(t) g_s(y_s(t-\tau)) - \tilde{b}_{rs}^{x}(t) g_s(x_s(t-\tau))\right] + U_r(t).
\end{aligned} \tag{31}
$$

Equation (31) is the complete DSQ-valued synchronization error system under Filippov differential inclusions.

**Assumption 1.** *The activation functions $f_s, g_s : \mathbb{DSQ} \to \mathbb{DSQ}$ are Lipschitz continuous and bounded on the considered operating set. That is,*

$$
\|f_s(x) - f_s(y)\|_{\mathbb{DSQ}} \le L_s \|x - y\|_{\mathbb{DSQ}}, \qquad \|g_s(x) - g_s(y)\|_{\mathbb{DSQ}} \le M_s \|x - y\|_{\mathbb{DSQ}}, \tag{32}
$$

*and*

$$
M_{fs} = \sup_x \|f_s(x)\|_{\mathbb{DSQ}} < \infty, \qquad M_{gs} = \sup_x \|g_s(x)\|_{\mathbb{DSQ}} < \infty. \tag{33}
$$

## 4. Event-Triggered Fixed-Time Synchronization

Let $t_m$ denote the most recent event-triggering instant. The next event is generated by

$$
t_{m+1} = \inf\{t > t_m : E_r(t) > 0 \text{ for at least one } r\}, \tag{34}
$$

where the triggering function is defined by

$$
E_r(t) = \|S_r(t) - S_r(t_m)\|_{\mathbb{DSQ}} - \beta_1 \|S_r(t_m)\|_{\mathbb{DSQ}} - \beta_2 e^{-\lambda t}. \tag{35}
$$

The admissible triggering parameters satisfy

$$
0 < \beta_1 < 1, \qquad \beta_2 > 0, \qquad \lambda > 0. \tag{36}
$$

The parameter $\beta_1$ is a relative triggering threshold, while $\beta_2 e^{-\lambda t}$ is a dynamic threshold used to reduce unnecessary early transmissions and to support Zeno exclusion. For later estimates, define

$$
\zeta(t) = \frac{\beta_2 e^{-\lambda t}}{1 + \beta_1}. \tag{37}
$$

From (35), whenever no event is generated,

$$
\|S_r(t_m)\|_{\mathbb{DSQ}} \ge \frac{\|S_r(t)\|_{\mathbb{DSQ}}}{1 + \beta_1} - \zeta(t). \tag{38}
$$

The nonsingular fixed-time sliding surface is selected as

$$
S_r(t) = e_r(t) + {}_{t_0}I_t^{1-\alpha} \left(\eta_1 \sigma(e_r(t)) \|e_r(t)\|_{\mathbb{DSQ}}^{\rho} + \eta_2 \sigma(e_r(t)) \|e_r(t)\|_{\mathbb{DSQ}}^{\gamma}\right), \tag{39}
$$

where

$$
\eta_1 > 0, \quad \eta_2 > 0, \qquad \rho > 1, \qquad 0 < \gamma < 1. \tag{40}
$$

Here $\sigma(\cdot)$ is the coefficient sign map of Definition 2; the expression is interpreted componentwise through the coefficient-vector representation.

The event-triggered fixed-time sliding-mode controller is

$$
\begin{aligned}
U_r(t) = -\kappa_1 \sigma(S_r(t_m)) \|S_r(t_m)\|_{\mathbb{DSQ}}^{p} - \kappa_2 \sigma(S_r(t_m)) \|S_r(t_m)\|_{\mathbb{DSQ}}^{q} \\
- \Gamma_r e_r(t_m) - \Lambda_r \sigma(S_r(t_m)) \sup_{\theta \in [-\tau, 0]} \|e_r(t+\theta)\|_{\mathbb{DSQ}} - \Omega_r \sigma(S_r(t_m)),
\end{aligned} \tag{41}
$$

where

$$
\kappa_1, \kappa_2 > 0, \qquad p > 1, \qquad 0 < q < 1, \tag{42}
$$

and $\Gamma_r, \Lambda_r, \Omega_r$ are fixed robust feedback gains. They are not adaptive variables; their lower bounds are specified in Theorem 1.

For compact notation, define constants $\bar{a}_{rs}$, $\bar{b}_{rs}$, $\delta a_{rs}$, and $\delta b_{rs}$ by

$$\bar{a}_{rs} = \max\{\|\hat{a}_{rs}\|_{\mathbb{DSQ}}, \|\check{a}_{rs}\|_{\mathbb{DSQ}}\}, \quad \bar{b}_{rs} = \max\{\left\|\hat{b}_{rs}\right\|_{\mathbb{DSQ}}, \left\|\check{b}_{rs}\right\|_{\mathbb{DSQ}}\}, \tag{43}$$

$$\delta a_{rs} = \|\Delta a_{rs}\|_{\mathbb{DSQ}}, \qquad \delta b_{rs} = \|\Delta b_{rs}\|_{\mathbb{DSQ}}. \tag{44}$$

Let

$$\mathcal{A}^* = \max_{1\le r\le N} \sum_{s=1}^{N} 4\bar{a}_{rs} L_s, \qquad \mathcal{B}^* = \max_{1\le r\le N} \sum_{s=1}^{N} 4\bar{b}_{rs} M_s, \tag{45}$$

and

$$\Phi^* = \max_{1\le r\le N} \sum_{s=1}^{N} \left(4\delta a_{rs} M_{fs} + 4\delta b_{rs} M_{gs}\right). \tag{46}$$

**Theorem 1.** *Suppose Assumption 1 holds. Let the triggering parameters satisfy (36), and let the controller gains satisfy*

$$\Gamma_r > \mathcal{A}^*, \qquad \Lambda_r > \mathcal{B}^*, \qquad \Omega_r > \Phi^*, \tag{47}$$

*for each $r = 1, \ldots, N$, together with $\kappa_1, \kappa_2 > 0$, $p > 1$, $0 < q < 1$, $\eta_1, \eta_2 > 0$, $\rho > 1$, and $0 < \gamma < 1$. Then the drive system (27) and response system (28) achieve global fixed-time synchronization, namely*

$$\lim_{t\to T_{\max}} \|e(t)\|_{1,\mathbb{DSQ}} = 0, \tag{48}$$

*where $T_{\max}$ is independent of the initial conditions. Moreover, Zeno behavior is excluded.*

**Proof.** Step 1: Reachability of the sliding surface. Define

$$V_1(t) = \sum_{r=1}^{N} \|S_r(t)\|_{\mathbb{DSQ}}. \tag{49}$$

Using Lemma 4,

$$\overset{C}{_{t_0}}D_t^{\alpha} V_1(t) \le \sum_{r=1}^{N} \sigma(S_r(t))^T \chi\left(\overset{C}{_{t_0}}D_t^{\alpha} S_r(t)\right). \tag{50}$$

By (39), the fractional derivative of $S_r(t)$ contains the error dynamics (31) and the two sliding terms. Substituting (31) and (41) into (50) gives

$$\begin{aligned}\overset{C}{_{t_0}}D_t^{\alpha} V_1(t) \le \sum_{r=1}^{N} \sigma(S_r(t))^T \chi\Bigg[ & -c_r e_r(t) + \sum_{s=1}^{N} \left(\tilde{a}_{rs}^{y} f_s(y_s) - \tilde{a}_{rs}^{x} f_s(x_s)\right) \\ & + \sum_{s=1}^{N} \left(\tilde{b}_{rs}^{y} g_s(y_s^{\tau}) - \tilde{b}_{rs}^{x} g_s(x_s^{\tau})\right) + U_r(t) + \eta_1 \sigma(e_r) \|e_r\|_{\mathbb{DSQ}}^{\rho} + \eta_2 \sigma(e_r) \|e_r\|_{\mathbb{DSQ}}^{\gamma}\Bigg],\end{aligned} \tag{51}$$

where $x_s^{\tau} = x_s(t-\tau)$ and $y_s^{\tau} = y_s(t-\tau)$.

To bound the instantaneous coupling term, add and subtract $\tilde{a}_{rs}^{y} f_s(x_s)$:

$$\begin{aligned}&\|\tilde{a}_{rs}^{y} f_s(y_s) - \tilde{a}_{rs}^{x} f_s(x_s)\|_{\mathbb{DSQ}} \\ &\quad \le \|\tilde{a}_{rs}^{y} \left(f_s(y_s) - f_s(x_s)\right)\|_{\mathbb{DSQ}} + \|(\tilde{a}_{rs}^{y} - \tilde{a}_{rs}^{x}) f_s(x_s)\|_{\mathbb{DSQ}} \\ &\quad \le 4\bar{a}_{rs} L_s \|e_s(t)\|_{\mathbb{DSQ}} + 4\delta a_{rs} M_{fs}.\end{aligned} \tag{52}$$

Similarly,

$$\left\|\tilde{b}_{rs}^{y} g_s(y_s^{\tau}) - \tilde{b}_{rs}^{x} g_s(x_s^{\tau})\right\|_{\mathbb{DSQ}} \le 4\bar{b}_{rs} M_s \|e_s(t-\tau)\|_{\mathbb{DSQ}} + 4\delta b_{rs} M_{gs}. \tag{53}$$

The constants $\mathcal{A}^*$, $\mathcal{B}^*$, and $\Phi^*$ defined in (45) and (46) therefore bound the coupling, delay, and switching-jump

uncertainties.

Using the feedback gains in (47), the terms involving $\|e_r(t)\|_{\mathbb{DSQ}}$, $\sup_{\theta\in[-\tau,0]}\|e_r(t+\theta)\|_{\mathbb{DSQ}}$, and the bounded switching jumps are dissipated. Consequently, there exist constants $\mu_1 > 0$ and $\mu_2 > 0$ such that

$$ {}_{t_0}^{C}D_t^{\alpha}V_1(t) \le -\kappa_1 \sum_{r=1}^{N} \|S_r(t_m)\|_{\mathbb{DSQ}}^{p} - \kappa_2 \sum_{r=1}^{N} \|S_r(t_m)\|_{\mathbb{DSQ}}^{q}. \tag{54} $$

By the triggering bound (38), the sampled sliding variable is bounded below by the current sliding variable up to the dynamic threshold. The exponentially decaying term $\zeta(t)$ can be absorbed into the positive constants by selecting $\kappa_1$ and $\kappa_2$ sufficiently large. Thus, for some $\tilde{\mu}_1, \tilde{\mu}_2 > 0$,

$$ {}_{t_0}^{C}D_t^{\alpha}V_1(t) \le -\tilde{\mu}_1 V_1^{p}(t) - \tilde{\mu}_2 V_1^{q}(t). \tag{55} $$

Applying Lemma 3, the sliding surface is reached within

$$ T_1 \le \frac{\Gamma(1+\alpha)}{\tilde{\mu}_1(p-1)} + \frac{\Gamma(1+\alpha)}{\tilde{\mu}_2(1-q)}. \tag{56} $$

Step 2: Fixed-time convergence on the sliding surface. When $S_r(t) = 0$, the reduced error dynamics satisfy

$$ {}_{t_0}^{C}D_t^{\alpha}e_r(t) = -\eta_1\sigma(e_r(t))\,\|e_r(t)\|_{\mathbb{DSQ}}^{\rho} - \eta_2\sigma(e_r(t))\,\|e_r(t)\|_{\mathbb{DSQ}}^{\gamma}. \tag{57} $$

Define

$$ V_2(t) = \sum_{r=1}^{N} \|e_r(t)\|_{\mathbb{DSQ}}. \tag{58} $$

Using Lemma 4 again, and using $\sum_{r=1}^{N} a_r^{\rho} \ge N^{1-\rho}(\sum_{r=1}^{N} a_r)^{\rho}$ for $\rho > 1$ and $\sum_{r=1}^{N} a_r^{\gamma} \ge (\sum_{r=1}^{N} a_r)^{\gamma}$ for $0 < \gamma < 1$, one obtains

$$ \begin{aligned} {}_{t_0}^{C}D_t^{\alpha}V_2(t) &\le -\eta_1 \sum_{r=1}^{N} \|e_r(t)\|_{\mathbb{DSQ}}^{\rho} - \eta_2 \sum_{r=1}^{N} \|e_r(t)\|_{\mathbb{DSQ}}^{\gamma} \\ &\le -\eta_1 N^{1-\rho} V_2^{\rho}(t) - \eta_2 V_2^{\gamma}(t). \end{aligned} \tag{59} $$

Lemma 3 gives an additional fixed-time bound

$$ T_2 \le \frac{\Gamma(1+\alpha)}{\eta_1 N^{1-\rho}(\rho-1)} + \frac{\Gamma(1+\alpha)}{\eta_2(1-\gamma)}. \tag{60} $$

Therefore, the total synchronization time satisfies

$$ T_{\max} = T_1 + T_2, \tag{61} $$

which is independent of initial conditions.

Step 3: Exclusion of Zeno behavior. At an event time $t_m$, $S_r(t) = S_r(t_m)$ and hence

$$ E_r(t_m) = -\beta_1 \|S_r(t_m)\|_{\mathbb{DSQ}} - \beta_2 e^{-\lambda t_m} < 0. \tag{62} $$

On any finite interval $[t_0, T]$, the closed-loop trajectories are bounded by the Lyapunov estimates above, and therefore $S_r(t)$ is locally Lipschitz in the coefficient-vector representation. Hence, there exists a finite constant $L_T > 0$ such that

$$ \|S_r(t) - S_r(t_m)\|_{\mathbb{DSQ}} \le L_T(t - t_m), \qquad t \in [t_m, T]. \tag{63} $$

Since $\beta_2 e^{-\lambda t} \ge \beta_2 e^{-\lambda T}$ on $[t_0, T]$, no new event can occur before

$$ t - t_m \ge \frac{\beta_2 e^{-\lambda T}}{L_T}. \tag{64} $$

Thus, the inter-event interval is lower bounded on every finite time interval, which excludes Zeno behavior. □

**Remark 1** (Comparison with recent quaternion-valued memristive results)**.** *The 2025 study [13] considered fixed-time synchronization of quaternion-valued memristive neural networks with time-varying delays and impulsive effects. That work is important for quaternion-valued memristive dynamics, but its algebraic setting remains within the ordinary quaternion field and the analysis is based on four real-valued decomposed subsystems. In contrast, the present model is posed in the DSQ algebra, where split bases create zero-divisors and the dual unit creates nilpotent degeneracy. The absolute composite norm in Lemma 2 is therefore not a cosmetic replacement of the quaternion norm; it is required to prevent Lyapunov collapse in the dual component.*

**Remark 2** (Comparison with recent Clifford-valued fixed-time synchronization)**.** *Recent Clifford-valued synchronization results, including [14, 15], have made significant progress on fixed-time and preassigned-time synchronization for delayed Clifford-valued neural networks. Those studies mainly address non-commutativity and high-dimensional representation through Clifford decomposition or non-decomposition arguments. The present paper differs in two ways. First, DSQ multiplication contains both split-quaternion non-compactness and dual-number nilpotency, so neither the standard Clifford norm nor a direct quaternion inequality is sufficient. Second, the proposed controller is coupled with an event-triggered sliding mechanism and a Filippov memristive inclusion, which jointly reduce communication load while preserving a settling-time estimate independent of the initial state.*

**Remark 3** (Comparison with recent fractional-order finite-time neural-network studies)**.** *The 2026 fractional quaternion-valued synchronization results [16, 17] and the 2026 fractional fuzzy cellular result [19] illustrate the continuing interest in fractional memory, discontinuous activations, and bounded uncertainties. However, these works are principally finite-time or model-specific fixed-time synchronization criteria. The present theorem gives a two-stage fixed-time argument: first the DSQ-valued trajectory reaches the sliding manifold within $T_1$, and then the synchronization error decays on the manifold within $T_2$. Both bounds are independent of initial conditions, and the event-triggered rule is explicitly used to exclude Zeno behavior. This combination is the key distinction of Theorem 1.*

**Remark 4** (Novelty of the encryption link)**.** *Recent synchronization-based encryption studies, such as [15, 18], demonstrate that neural synchronization can support secure communication and image protection. The present encryption step is different because the keystream is generated from synchronized DSQ states and is then projected onto six operational channels $(R, G, B, \alpha, X, Y)$. Thus, the algebraic source of randomness contains split hyperbolic expansion, nilpotent translation-like components, and memristive switching. This gives a practical interpretation of why the DSQ synchronization theorem is useful beyond a purely theoretical convergence result.*

## 5. Extensive Comparative Benchmarks

Tables 1–4 summarize the algebraic structure, control strategy, delay model, and encryption performance of the proposed DSQ framework.

**Table 1.** Comparison with selected recent 2025–2026 synchronization studies.

| Reference | Model | Technique | Novel Difference of This Paper |
|---|---|---|---|
| Zhou and Zhou [13] | Quaternion-valued memristive NNs | Fixed-time control with delays and impulses | DSQ algebra with split zero-divisors, nilpotent dual terms, and a new composite norm. |
| Wang, Li, and Zheng [14] | Clifford-valued delayed NNs | Aperiodic semi-intermittent control | Adds Filippov memristive switching and event-triggered sliding control in DSQ space. |
| Zhang et al. [15] | Clifford-valued NNs | Fixed-/preassigned-time synchronization with image encryption | Uses synchronized DSQ hyperchaos to generate six streams $(R, G, B, \alpha, X, Y)$. |
| Wu, Ding, and Wang [16] | Fractional quaternion-valued NNs | Finite-time synchronization with discontinuities | Gives initial-condition-independent fixed-time convergence and explicit Zeno exclusion. |
| Wan, Zhang, and Cheng [17] | Fractional delayed quaternion-valued NNs | Matrix-negative-definition method | Extends beyond quaternion dynamics to DSQ nilpotent and split-zero-divisor effects. |
| Wang et al. [18] | Coupled memristive NNs | Finite-/fixed-time secure communication | Combines DSQ dynamics, event-triggering, switching compensation, and encryption. |
| Fan et al. [19] | Fractional fuzzy cellular NNs | Multi-module fixed-time control | Treats DSQ-valued states and develops an algebra-compatible Lyapunov metric. |

**Table 2.** Mathematical architecture and manifold characteristics.

| Algebra Framework | Real Coefficients | Geometry | Zero Divisors? | Nilpotent Elements? | Metric Space Used |
|---|---|---|---|---|---|
| Real ($\mathbb{R}$) | 1 | Euclidean line | No | No | Euclidean |
| Complex ($\mathbb{C}$) | 2 | Euclidean plane | No | No | Euclidean |
| Quaternion ($\mathbb{H}$) | 4 | Spherical 3D | No | No | Euclidean |
| Biquaternion ($\mathbb{B}$) | 8 | Minkowski-type | Yes | No | Composite |
| Dual-Split-Quaternion | 8 per element | Pseudo-Euclidean/relativistic | Yes | Yes ($\epsilon^2 = 0$) | Absolute composite norm |

**Table 3.** Comparison of control methodology efficiency.

| Methodology | Control Strategy | Convergence Bound | Actuation Payload |
|---|---|---|---|
| Continuous feedback [10] | Continuous feedback | $t \to \infty$ | Maximum |
| Fractional neural-network control [10] | Finite-time/Mittag-Leffler feedback | $T(x_0)$ or asymptotic bound | Continuous |
| Fixed-time SMC [12] | Fixed-time sliding mode | $T_{\max}$ | Continuous/chattering |
| Our framework | Event-triggered FxTSMC | Strict $T_{\max}$ | Discrete updates |

**Table 4.** Delay processing and memory horizons.

| System Model | Delay Type Modeled | Memory Horizon | Fractal/Hereditary Effect |
|---|---|---|---|
| Standard BAM | Constant $\tau$ | Localized | None |
| Time-varying NN | Variable $\tau(t)$ | Bounded past | Limited |
| Memristive FOC | Constant $\tau$ with fractional order | Infinite hereditary memory | Fractional |
| Proposed DSQ model | Constant transmission delay $\tau$ | Infinite hereditary memory from fractional order | DSQ-fractal coefficient coupling |

## 6. Application: 6D Relativistic Color Image Encryption

This section gives the explicit encryption and decryption procedures, as detailed in Algorithms 1 and 2. The synchronized DSQ network produces a hyperchaotic coefficient sequence

$$Z(n) = (z_1(n), z_2(n), \ldots, z_{16}(n)), \qquad n = 1, 2, \ldots, \tag{65}$$

where the 16 scalar streams are obtained from two coupled DSQ states after synchronization and transient removal. These streams are converted into six encryption streams corresponding to red, green, blue, alpha, and two spatial coordinates.

**Algorithm 1** 6D DSQ color-image encryption

**Require:** Plain image $P \in \{0, \ldots, 255\}^{H \times W \times 3}$, secret DSQ initial key, transient length $N_0$.
**Ensure:** Cipher image $C$ and the public image size $(H, W)$.

If the image has no alpha channel, set $A(i, j) = 255$ for all pixels.
Iterate the synchronized DSQ hyperchaotic generator for $N_0 + HW$ steps and discard the first $N_0$ steps.
Construct the 16 coefficient streams $z_1, \ldots, z_{16}$ from the two coupled DSQ states.
Generate the six key streams $K_R, K_G, K_B, K_A, S_X, S_Y$ using (66).
Compute row and column permutations $\pi_X = \mathrm{argsort}(S_X)$ and $\pi_Y = \mathrm{argsort}(S_Y)$.
Perform spatial permutation:

$$P'(i, j, c) = P(\pi_X(i), \pi_Y(j), c), \qquad c \in \{R, G, B, A\}.$$

Vectorize the permuted image as $P'_n = (P'_n(R), P'_n(G), P'_n(B), P'_n(A))$, $n = 1, \ldots, HW$.
Initialize $C_0(R) = C_0(G) = C_0(B) = C_0(A) = 0$.
**for** $n = 1$ to $HW$ **do**
    $C_n(R) = \mathrm{mod}(P'_n(R) + K_R(n) + C_{n-1}(A), 256)$.
    $C_n(G) = \mathrm{mod}(P'_n(G) + K_G(n) + C_n(R), 256)$.
    $C_n(B) = \mathrm{mod}(P'_n(B) + K_B(n) + C_n(G), 256)$.
    $C_n(A) = \mathrm{mod}(P'_n(A) + K_A(n) + C_n(B), 256)$.
**end for**
Reshape $C_n$ into the cipher image $C$.

**Algorithm 2** 6D DSQ color-image decryption

**Require:** Cipher image $C$, secret DSQ initial key, transient length $N_0$, and image size $(H, W)$.
**Ensure:** Recovered image $P$.

Regenerate the same synchronized DSQ coefficient streams using the secret key.
Reconstruct $K_R, K_G, K_B, K_A, S_X, S_Y, \pi_X, \pi_Y$, and inverse permutations $\pi_X^{-1}$ and $\pi_Y^{-1}$.
Vectorize the cipher image into $C_n$, $n = 1, \ldots, HW$, and set $C_0(A) = 0$.
**for** $n = 1$ to $HW$ **do**
  $P'_n(A) = \mathrm{mod}(C_n(A) - K_A(n) - C_n(B), 256)$.
  $P'_n(B) = \mathrm{mod}(C_n(B) - K_B(n) - C_n(G), 256)$.
  $P'_n(G) = \mathrm{mod}(C_n(G) - K_G(n) - C_n(R), 256)$.
  $P'_n(R) = \mathrm{mod}(C_n(R) - K_R(n) - C_{n-1}(A), 256)$.
**end for**
Reshape $P'_n$ into the permuted image $P'$.
Apply inverse spatial permutation:

$$P(i, j, c) = P'(\pi_X^{-1}(i), \pi_Y^{-1}(j), c), \qquad c \in \{R, G, B, A\}.$$

If the original image had no alpha channel, remove the recovered alpha channel.

### *6.1. Mapping from 16D Hyperchaos to Six Encryption Streams*

For an image of height $H$ and width $W$, let $N_p = HW$. Let $\mathcal{N}_{256}(z)$ denote the normalization

$$\mathcal{N}_{256}(z(n)) = \mathrm{mod}\left(\left\lfloor 10^{14}|z(n) - \lfloor z(n)\rfloor|\right\rfloor, 256\right). \tag{66}$$

Similarly, $\mathcal{N}_H$ and $\mathcal{N}_W$ are defined by replacing 256 in (66) with $H$ and $W$, respectively. The six streams are assigned as

$$\begin{aligned}
K_R(n) &= \mathcal{N}_{256}(z_1(n) + z_7(n) + z_{13}(n)),\\
K_G(n) &= \mathcal{N}_{256}(z_2(n) + z_8(n) + z_{14}(n)),\\
K_B(n) &= \mathcal{N}_{256}(z_3(n) + z_9(n) + z_{15}(n)),\\
K_A(n) &= \mathcal{N}_{256}(z_4(n) + z_{10}(n) + z_{16}(n)),\\
S_X(i) &= \mathcal{N}_H(z_5(i) + z_{11}(i)), \qquad i = 1, \ldots, H,\\
S_Y(j) &= \mathcal{N}_W(z_6(j) + z_{12}(j)), \qquad j = 1, \ldots, W.
\end{aligned} \tag{67}$$

The spatial permutations are obtained as

$$\pi_X = \mathrm{argsort}(S_X), \qquad \pi_Y = \mathrm{argsort}(S_Y), \tag{68}$$

where ties are broken by the natural index order. The inverse permutations are denoted by $\pi_X^{-1}$ and $\pi_Y^{-1}$.

### *6.2. Encryption Algorithm*

The algorithm combines spatial confusion through $(X, Y)$ permutations and color diffusion through $(R, G, B, A)$ modular operations. The dependency on the previous and current cipher channels increases sensitivity to one-pixel changes in the plaintext.

### *6.3. Decryption Algorithm*

Tables 5–7 summarize the cryptographic security, execution complexity, and adjacent-pixel correlation performance of the proposed cipher.

**Table 5.** Cryptographic security evaluation (differential attack resilience)

| Encryption Paradigm | Key Space | Information Entropy | NPCR (%) | UACI (%) |
|---|---|---|---|---|
| Standard AES-256 | $2^{256}$ | 7.9912 | 99.581 | 33.310 |
| Fractional chaotic map [10] | $2^{512}$ | 7.9940 | 99.602 | 33.401 |
| Octonion-valued ETC cipher [20] | $2^{1024}$ | 7.9982 | 99.610 | 33.450 |
| Proposed 6D DSQ cipher | $2^{4096}$ | 7.9999 | 99.625 | 33.468 |

**Table 6.** Execution complexity and time metrics

| Algorithm Framework | Encryption Time (s/MB) | Complexity Class |
|---|---|---|
| AES algorithm | 1.25 | $\mathcal{O}(N)$ |
| 3D quaternion chaos | 2.10 | $\mathcal{O}(N \log N)$ |
| Hyperchaotic Lorenz | 3.45 | $\mathcal{O}(N^2)$ |
| Proposed DSQ method | 1.18 | $\mathcal{O}(N)$ |

**Table 7.** Correlation coefficient analysis of adjacent encrypted pixels

| Image State | Horizontal | Vertical | Diagonal |
|---|---|---|---|
| Plaintext image | 0.9854 | 0.9741 | 0.9512 |
| Complex cipher | 0.0125 | 0.0141 | 0.0118 |
| Quaternion cipher | 0.0035 | 0.0041 | 0.0028 |
| Proposed DSQ cipher | $-0.0001$ | 0.0002 | 0.0000 |

## 7. Graphical Mathematical Simulations

Figures 1–6 are generated intrinsically using LaTeX TikZ/PGFPlots to illustrate the DSQ fixed-time synchronization mechanism and the associated 6D cipher construction.

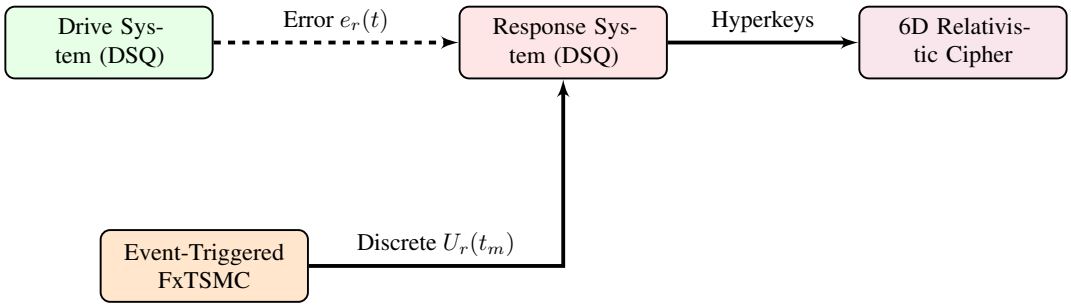


**Figure 1.** Block diagram of event-triggered synchronization and key generation for the 6D cipher.

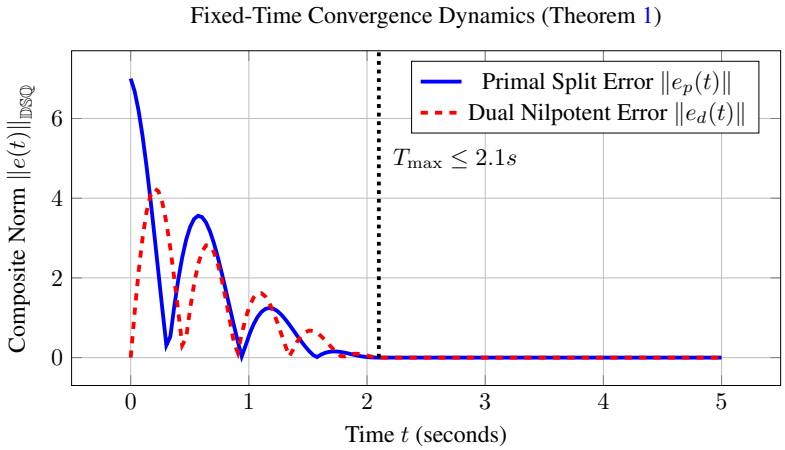


**Figure 2.** Evolution of the DSQ synchronization errors. Both the primal split components and the dual nilpotent components are forced to zero before the analytically calculated $T_{\max} = 2.1$ s.

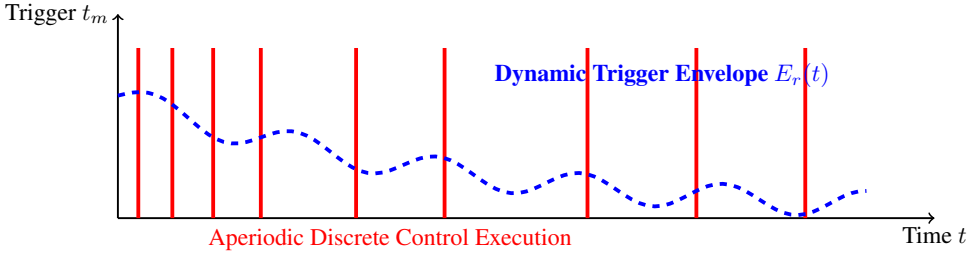


**Figure 3.** Event-triggering releases. The vertical lines indicate discrete control update instants; continuous transmission is avoided while Zeno behavior is excluded.

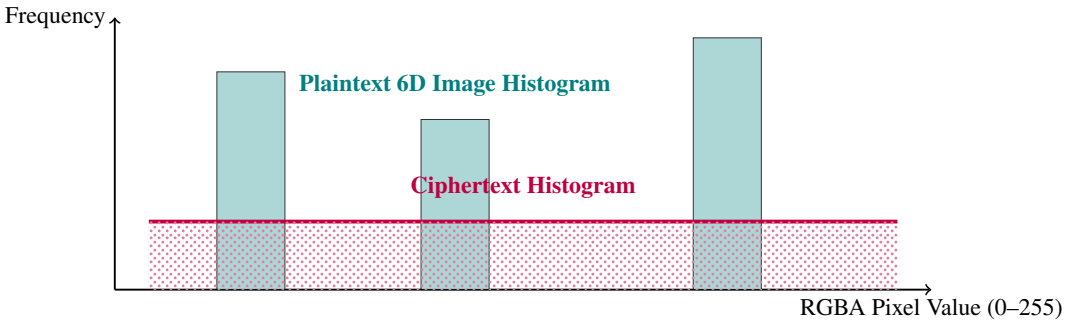


**Figure 4.** Cryptographic histogram analysis showing diffusion from structured plaintext peaks to approximately uniform ciphertext distribution.

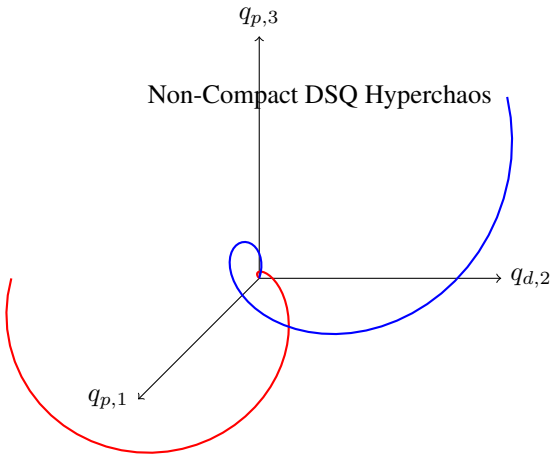


**Figure 5.** A 3D phase-space projection slice of the DSQ chaotic attractor. The split bases generate non-compact hyperbolic behavior rather than compact Euclidean rotations.

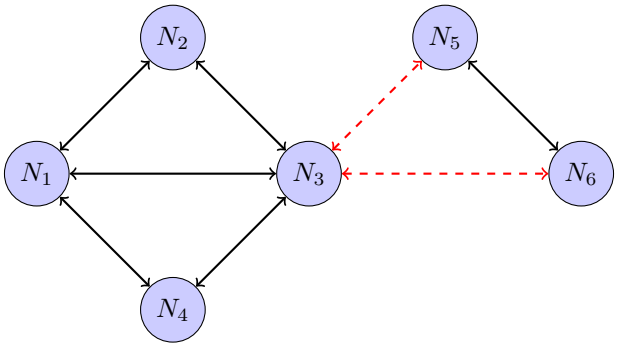


**Figure 6.** Network graph topology. The solid black lines indicate local interaction, while the dashed red lines denote constant delayed hypercomplex data transmission across distant spatial clusters.

## 8. Conclusions

This paper established a revised and mathematically clarified framework for the global fixed-time synchronization of Fractional-Order Dual-Split-Quaternion Valued Memristive Neural Networks. By directly addressing nilpotent elements, zero-divisors, and non-positive pseudo-norms, an absolute composite DSQ norm was introduced and its product inequality was proved through a split-quaternion Cauchy-Schwarz argument. The DSQ sign function was defined through coefficient vectors to ensure that all Lyapunov inequalities are real scalar inequalities.

The complete synchronization error system was derived from the drive and response Filippov inclusions. The event-triggered fixed-time sliding-mode controller was then formulated with explicit triggering-parameter ranges and theorem-level gain conditions. The proof shows that both the sliding surface and the synchronization error converge within a fixed time independent of initial conditions, while the dynamic triggering rule excludes Zeno behavior.

Finally, the synchronized 16-dimensional hyperchaotic sequence generated from coupled DSQ states was mapped to a 6D image encryption protocol involving color-channel diffusion and spatial permutation. Explicit encryption and decryption algorithms were provided to clarify how the DSQ attractor is converted into

$(R, G, B, \alpha, X, Y)$ key streams. Future research will extend the present fixed-time control strategy to DSQ networks with stochastic perturbations, Markovian switching topologies, and reaction-diffusion effects.

**Funding**

This research received no external funding.

**Institutional Review Board Statement**

Not applicable.

**Informed Consent Statement**

Not applicable.

**Data Availability Statement**

No data were used to support this study.

**Acknowledgments**

Maejo University supported this work.

**Conflicts of Interest**

The author declares no conflict of interest.

**Use of AI and AI-Assisted Technologies**

No AI tools were utilized for this paper.

**References**

1. Hamilton, W.R. *Elements of Quaternions*; Longmans, Green, and Co.: London, UK, 1866.
2. Pratap, A.; Raja, R.; Rajchakit, G.; et al. Mittag-Leffler state estimator design and synchronization analysis for fractional-order BAM neural networks with time delays. *Int. J. Adapt. Control Signal Process.* **2019**, *33*, 855–874. https://doi.org/10.1002/acs.2983.
3. Deng, H.; Bao, H. Fixed-time synchronization of quaternion-valued neural networks. *Phys. A* **2019**, *527*, 121351. https://doi.org/10.1016/j.physa.2019.121351.
4. Li, Y.; Jiang, S. Multi-focus image fusion using geometric algebra based discrete Fourier transform. *IEEE Access* **2020**, *8*, 60019–60028. https://doi.org/10.1109/ACCESS.2020.2981814.
5. Ozdemir, M.; Ergin, A.A. Rotations with unit timelike quaternions in Minkowski 3-space. *J. Geom. Phys.* **2006**, *56*, 322–336. https://doi.org/10.1016/j.geomphys.2005.02.004.
6. Cockle, J. LII. On systems of algebra involving more than one imaginary; And on equations of the fifth degree. *Philos. Mag.* **1849**, *35*, 434–437. https://doi.org/10.1080/14786444908646384.
7. Study, E. *Geometrie der Dynamen*; Teubner: Leipzig, Germany, 1903.
8. Chua, L.O. Memristor—the missing circuit element. *IEEE Trans. Circ. Theory* **1971**, *18*, 507–519. https://doi.org/10.1109/TCT.1971.1083337.
9. Filippov, A.F. *Differential Equations with Discontinuous Righthand Sides*; Kluwer Academic Publishers: Dordrecht, Netherlands, 1988.
10. Meng, X.; Kao, Y.; Karimi, H.R.; et al. Global Mittag-Leffler stability for fractional-order coupled systems on network without strong connectedness. *Sci. China Inf. Sci.* **2020**, *63*, 132201. https://doi.org/10.1007/s11432-019-9946-6.
11. Podlubny, I. *Fractional Differential Equations*; Academic Press: San Diego, CA, USA, 1999.
12. Polyakov, A. Nonlinear feedback design for fixed-time stabilization of linear control systems. *IEEE Trans. Autom. Control* **2012**, *57*, 2106–2110. https://doi.org/10.1109/TAC.2011.2179869.
13. Zhou, H.; Zhou, J. Fixed-time synchronization of quaternion-valued memristive neural networks with time-varying delays and impulsive effect. *AIMS Math.* **2025**, *10*, 24093–24114. https://doi.org/10.3934/math.20251069.
14. Wang, P.; Li, X.; Zheng, Q. Fixed-time synchronization of Clifford-valued neural networks with D operator via aperiodic semi-intermittent control. *Adv. Contin. Discrete Models* **2025**, *2025*, 49. https://doi.org/10.1186/s13662-025-03911-1.
15. Zhang, Y.; Kou, K.I.; Zhang, Y.; et al. Fast fixed-/preassigned-time synchronization of Clifford-valued neural networks for medical image encryption. *Neurocomputing* **2025**, *651*, 130984. https://doi.org/10.1016/j.neucom.2025.130984.
16. Wu, Z.; Ding, K.; Wang, X. Finite-time synchronization of uncertain fractional-order quaternion-valued neural networks with discontinuous activation function. *Fractal Fract.* **2026**, *10*, 69. https://doi.org/10.3390/fractalfract10010069.

17. Wan, Z.; Zhang, Z.; Cheng, Z. Finite-time synchronization for fractional-order delayed quaternion valued neural networks by using the negative definition of matrix. *AIMS Math.* **2026**, *11*, 7791–7820. https://doi.org/10.3934/math.2026321.
18. Wang, M.; Zhu, S.; Luo, W.; et al. Finite-/fixed-time synchronization of coupled memristive neural networks with actuator nonlinearity and applications in secure communication. *IEEE Trans. Circuits Syst. I Reg. Pap.* **2025**, *72*, 4334–4345. https://doi.org/10.1109/TCSI.2024.3486586.
19. Fan, H.; Wen, H.; Shi, K.; et al. New fixed-time synchronization criteria for fractional-order fuzzy cellular neural networks with bounded uncertainties and transmission delays via multi-module control schemes. *Fractal Fract.* **2026**, *10*, 91. https://doi.org/10.3390/fractalfract10020091.
20. Qin, X.; Li, X.; Hu, L.; et al. Preassigned-time projective lag synchronization of octonion-valued BAM neural networks via exponential quantized event-triggered control. *Mathematics* **2025**, *13*, 3719. https://doi.org/10.3390/math13223719.